Biol. Chem., Vol. 387, pp. 1063–1074, August 2006 • Copyright © by Walter de Gruyter • Berlin • New York. DOI 10.1515/BC.2006.131

Development of a red-shifted fluorescence-based assay for SARS-coronavirus 3CL protease: identification of a novel class of anti-SARS agents from the tropical marine sponge *Axinella corrugata*

Pamela Hamill[1], Derek Hudson[2], Richard Y. Kao[3], Polly Chow[1], Meera Raj[1], Hongyan Xu[4], Martin J. Richer[1] and François Jean[1,*]

[1] Department of Microbiology and Immunology, Life Sciences Centre, University of British Columbia, 3559-2350 Health Sciences Mall, Vancouver, BC V6T 1Z3, Canada

[2] Biosearch Technologies Inc., Novato, CA 94949-5750, USA

[3] Department of Microbiology, University of Hong Kong, Hong Kong SAR, China

[4] GL Biochem Ltd., Shanghai 201203, China

* Corresponding author
e-mail: fjean@interchange.ubc.ca

Abstract

SARS-coronavirus (SARS-CoV) encodes a main protease, 3CL^{pro}, which plays an essential role in the viral life cycle and is currently the prime target for discovering new anti-coronavirus agents. In this article, we report our success in developing a novel red-shifted (RS) fluorescence-based assay for 3CL^{pro} and its application for identifying small-molecule anti-SARS agents from marine organisms. We have synthesised and characterised the first generation of a red-shifted internally quenched fluorogenic substrate (RS-IQFS) for 3CL^{pro} based on resonance energy transfer between the donor and acceptor pair CAL Fluor Red 610 and Black Hole Quencher-1 (K_m and k_{cat} values of 14 μM and 0.65 min^{-1}). The RS-IQFS primary sequence was selected based on the results of our screening analysis of 3CL^{pro} performed using a series of blue-shifted (BS)-IQFSs corresponding to the 3CL^{pro}-mediated cleavage junctions of the SARS-CoV polyproteins. In contrast to BS-IQFSs, the RS-IQFS was not susceptible to fluorescence interference from coloured samples and allowed for successful screening of marine natural products and identification of a coumarin derivative, esculetin-4-carboxylic acid ethyl ester, a novel 3CL^{pro} inhibitor (IC_{50}=46 μM) and anti-SARS agent (EC_{50}=112 μM; median toxic concentration >800 μM) from the tropical marine sponge *Axinella corrugata*.

Keywords: fluorescence-based protease assay; internally quenched fluorogenic peptide substrate; SARS-coronavirus 3CL protease; viral protease; viral protease inhibitor.

Introduction

Since the emergence of severe acute respiratory syndrome in late 2002, its etiological agent, the novel SARS-coronavirus (SARS-CoV) (Drosten et al., 2003; Ksiazek et al., 2003), has been the subject of intense study aimed at understanding its pathogenesis and the development of novel therapies to treat infection. In common with other coronaviruses, the genome of SARS-CoV is a single-stranded, positive-sense RNA that is translated in the cytoplasm of infected cells. Among the viral gene products are the large polyproteins, pp1a and pp1b (Marra et al., 2003; Rota et al., 2003; Snijder et al., 2003; Thiel et al., 2003). These polyproteins must be proteolytically processed to generate the individual proteins required for viral replication to occur, a process that is mediated by two viral cysteine proteases: PL^{pro} (papain-like protease) (Lindner et al., 2005) and 3CL^{pro} (3C-like protease), which is also called the main protease (Ziebuhr, 2004; Liang, 2006). 3CL^{pro} is considered the main viral protease since, by analogy with other coronaviruses, it is responsible for releasing the key replicative proteins of the virus, including the viral RNA polymerase and helicase proteins. A total of 11 junctions within the SARS-CoV polyproteins are predicted to be cleaved by 3CL^{pro} (Marra et al., 2003; Rota et al., 2003; Snijder et al., 2003; Thiel et al., 2003), releasing the non-stuctural proteins (nsp) 5–16, which are thought to form a membrane-associated replicase complex that mediates transcription and replication of the viral genome (Snijder et al., 2006).

Since it plays such a crucial putative role in the viral life cycle, 3CL^{pro} is currently the main focus for development of SARS-CoV therapies. So far, an important biological role for SARS-CoV-encoded cysteine proteases in viral replication has been supported by the results of one study in which the replication of recombinant full-length infectious cDNA clones of the SARS virus was inhibited by treatment with a cysteine protease inhibitor, E64-d [(2*S*,3*S*)-transepoxysuccinyl-L-leucylamido-3-methylbutane ethyl ester] (Yount et al., 2003). Importantly, the availability of a SARS-CoV infectious clone now provides the tool needed to dissect, by genetic manipulation of the replicase gene, the biological role of 3CL^{pro} during viral replication (Yount et al., 2003).

Much progress has been made so far, and efforts have been accelerated by applying existing knowledge regarding the structure and function of homologous proteases in other human coronaviruses, such as strain 229E (Anand et al., 2003). SARS 3CL^{pro} (MEROPS designation C30.005) is a chymotrypsin-like protease, with the active site comprising a catalytic dyad of Cys145 and His41

residues rather than a triad (Anand et al., 2003). In common with the 3CL^{pro} structures from other coronaviruses previously reported (Anand et al., 2002), SARS-CoV 3CL^{pro} has three domains (Anand et al., 2003; Yang et al., 2003). Catalytic domains I and II form a chymotrypsin fold, while the third is an α-helical dimerisation domain that includes a critical C-terminal segment (approx. 100 residues) essential for dimerisation of 3CL^{pro} and its enzymatic activity (Shi et al., 2004). Interestingly, the results of a recent mutational study demonstrated that only one active protomer in the dimer is sufficient for SARS-CoV 3CL^{pro} catalysis (Chen et al., 2006).

Substrate specificity studies based on a HPLC method have confirmed that recombinant SARS 3CL^{pro} can proteolytically process dodecapeptidyl substrates (P6–P6′) covering all the 11 predicted pp1a and pp1b cleavage junctions *in vitro* (Fan et al., 2004). SARS-CoV 3CL^{pro} was shown to cleave the peptidyl substrates tested with different performance constants (k_{cat}/K_m) and cleavage of all the substrates occurred at the expected site, following the Gln residue in the conserved sequence of (Leu, Met, Phe, Val)-Gln↓-(Ser, Ala, Gly) at positions P2, P1, and P1′, respectively. The two peptides corresponding to the N- and C-termini self-cleavage sites of 3CL^{pro} were the best substrates. A more detailed study of SARS-CoV 3CL^{pro} substrate specificity was recently performed using a series of 34 synthetic peptides. Amino acids at position P3, P4, and P3′ of the scissile peptide bond were also found to be critical for substrate recognition and binding, suggesting a complex molecular interplay between the substrate-binding subsites and the Cys-His catalytic dyad (Fan et al., 2005).

A priority for generating novel 3CL^{pro} inhibitors is the development of sensitive assays to detect recombinant 3CL^{pro} activity in formats amenable to high-throughput screening. To date, several assay systems have been described to detect 3CL^{pro} activity, and these have allowed important inhibitor screening efforts to be undertaken (Liang, 2006). However, there is still knowledge to be gained regarding the development of an optimal substrate for this purpose.

We set out to develop a continuous fluorescence resonance energy transfer (FRET)-based assay that would allow enzymatic characterisation of recombinant 3CL^{pro} and allow reliable and fast screening of compound libraries for identifying 3CL^{pro} inhibitors. To this end, we first developed a series of internally consistent sets of decapeptidyl fluorescent substrates derived from the SARS-CoV 3CL^{pro}-dependent polyprotein cleavage sites to determine the optimal sequence for continuous monitoring of 3CL^{pro} activity. We then explored the effect of different fluorescent donor and acceptor pairs on the suitability of substrates for screening purposes. Substrates containing blue- or red-shifted fluorophores were assessed, since it has been recognised in recent years that fluorophores with emission maxima within the red region of the spectrum may be less susceptible to non-specific interference from coloured compounds than blue-shifted fluorophores (Grant et al., 2002; George et al., 2003).

Once a reliable FRET-based assay was established, we applied it to the screening of natural compounds derived from marine organisms for 3CL^{pro} inhibitory properties. Using this approach, we identified a novel, naturally occurring inhibitor of recombinant 3CL^{pro} activity *in vitro*, esculetin-4-carboxylic acid ethyl ester (MC8), derived from the marine sponge *Axinella corrugata*. Furthermore, using cell culture-based assays, we also demonstrated that MC8 is an effective inhibitor of SARS-CoV replication in Vero cells and that it mediates these effects at non-cytotoxic concentrations.

Results

Expression and purification of His-tagged SARS-CoV 3CL protease

To generate a sufficient amount of SARS-CoV 3CL^{pro} protease for the proposed comparative kinetic studies, we expressed His-tagged 3CL^{pro} protein in *Escherichia coli* and purified the soluble recombinant protein from clarified cell lysate by Ni^{2+} binding chromatography (Figure 1). This procedure yielded recombinant proteases that were essentially pure (>95%) and intact, as determined by Coomassie blue staining (Figure 1). The molecular composition of each preparation used in this study was confirmed by amino acid analysis (data not shown).

Design and synthesis of blue- and red-shifted internally quenched fluorogenic substrates (IQFSs) for SARS-CoV 3CL protease

Based upon the predicted 3CL^{pro}-mediated cleavage junctions within the SARS-CoV pp1a and pp1ab polyproteins, we designed an internally consistent set of decapeptidyl IQFSs to detect 3CL^{pro} activity *in vitro*

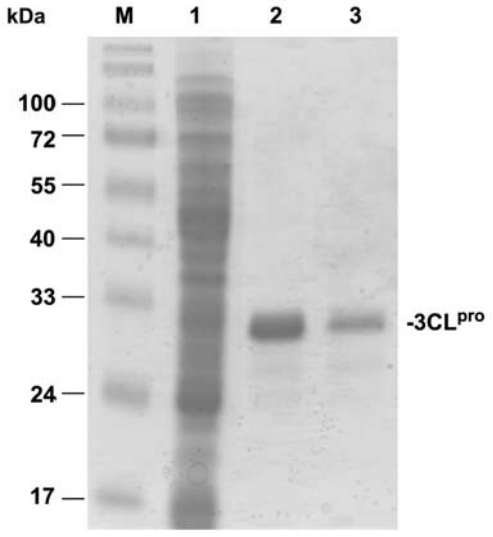

Figure 1 Purification of SARS-CoV 3CL protease.
Samples from stages during the expression and purification of 3CL^{pro} were analysed on a 12% SDS-polyacrylamide gel and stained using Coomassie Brilliant Blue. The lane marked M contains protein molecular weight markers; lane 1, lysate from BL21 *E. coli* induced to express 3CL^{pro}; lane 2, pooled peak fractions containing 3CL^{pro} eluted from the Ni^{2+} column using an imidazole gradient; lane 3, pooled peak fractions following dialysis against buffer C (see the materials and methods section).

Table 1 Internally quenched fluorogenic substrates (IQFS) for SARS-CoV 3CL^{pro}.

Peptide name		P6	P5	P4	P3	P2	P1		P1′	P2′	P3′	P4′		pp1a/b cleavage junction
BS-01	Abz	T	S	A	V	L	**Q**	–	**S**	G	F	R	$Y(NO_2)G\text{-}NH_2$	nsp4/nsp5
BS-02	Abz	S	G	V	T	F	**Q**	–	**G**	K	F	K	$Y(NO_2)G\text{-}NH_2$	nsp5/nsp6
BS-03	Abz	K	V	A	T	V	**Q**	–	**S**	K	M	S	$Y(NO_2)G\text{-}NH_2$	nsp6/nsp7
BS-04	Abz	N	R	A	T	L	**Q**	–	**A**	I	A	S	$Y(NO_2)G\text{-}NH_2$	nsp7/nsp8
BS-05	Abz	S	A	V	K	L	**Q**	–	**N**	N	E	L	$Y(NO_2)G\text{-}NH_2$	nsp8/nsp9
BS-06	Abz	A	T	V	R	L	**Q**	–	**A**	G	N	A	$Y(NO_2)G\text{-}NH_2$	nsp9/nsp10
BS-07	Abz	R	E	P	L	M	**Q**	–	**S**	A	D	A	$Y(NO_2)G\text{-}NH_2$	nsp10/nsp11
BS-08	Abz	P	H	T	V	L	**Q**	–	**A**	V	G	A	$Y(NO_2)G\text{-}NH_2$	nsp12/nsp13
BS-09	Abz	N	V	A	T	L	**Q**	–	**A**	E	N	V	$Y(NO_2)G\text{-}NH_2$	nsp13/nsp14
BS-10	Abz	T	F	T	R	L	**Q**	–	**S**	L	E	N	$Y(NO_2)G\text{-}NH_2$	nsp14/nsp15
BS-11	Abz	F	Y	P	K	L	**Q**	–	**A**	S	Q	A	$Y(NO_2)G\text{-}NH_2$	nsp15/nsp16
RS-01	CAL Fluor Red 610	T	S	A	V	L	**Q**	–	**S**	G	F	R	$K(BHQ\text{-}1)\text{-}NH_2$	nsp4/nsp5
RS-01 STD^{Nt}	CAL Fluor Red 610	T	S	A	V	L	Q	–	COOH					

The names, amino acid sequences, N-terminal fluorophore groups, C-terminal quenching moieties, and junctions within SARS-CoV polyproteins to which each peptide corresponds are listed for each IQFS. The residues in bold designate the predicted SARS-CoV 3CL^{pro} cleavage site (Ziebuhr, 2004).

(Table 1) (Ziebuhr, 2004). Each peptide substrate comprises a 10-residue sequence corresponding to one of the 11 predicted junctions within the polyprotein and is characterised by a fluorescent donor group at the N-terminus and an acceptor, or quenching, group at the C-terminus (Figure 2). We utilised two different sets of fluorescent donor and acceptor pairs: *O*-aminobenzoyl (Abz)/3-nitro-tyrosine [Y(3-NO_2)] (Jean et al., 1995) and CAL Fluor Red 610/Black hole quencher 1 (BHQ-1) (www.biosearchtech.com) (Figure 2). The two fluorophores exhibit peak emissions in different regions within the spectrum, with Abz and CAL Fluor Red 610 representing blue- and red-shifted fluorophores, respectively (Figures 2 and 5). The sequences of blue- and red-shifted IQFSs are shown in Table 1. When intact, resonance energy transfer between the fluorophore donor and acceptor moieties within the peptide results in quenching of the fluorescent energy. However, upon cleavage of any of the peptide bonds linking the two groups, the quenching effect is lost and an increase in fluorescence emission is observed. We and others have previously reported successful use of the Abz/Tyr (3-NO_2) combination for fluorogenic substrates (Jean et al., 1995; Richer et al., 2004; Hamill and Jean, 2005). However, to the best of our knowledge, this is the first time that CAL Fluor Red 610 and BHQ-1 have been utilised as a fluorophore/quencher pair in a fluorogenic peptide substrate, although BHQ groups are routinely used as quencher groups within DNA oligonucleotide probes (Wilson and Johansson, 2003; Boguszewska-Chachulska et al., 2004; Johansson et al., 2004; Moreira et al., 2005). With the exception of BS-09, all peptides were purified to a sufficiently high degree of homogeneity for use in this study. Despite several attempts, it was not possible to purify BS-09.

Processing of blue-shifted IQFSs by SARS-CoV 3CL^{pro}

All 10 BS-IQFSs were screened using an RP-HPLC assay to determine which peptides were processed by recombinant 3CL^{pro} *in vitro*. Protease assay reactions containing 50 μM of each BS-IQFS were resolved by RP-HPLC, and fluorescent peptide products were monitored to identify new fluorescent N-terminal peptides generated following incubation with 3CL^{pro}. Representative chromatograms showing the resolution of fluorescent peptide species within reactions containing each BS-IQFS are shown in Figure 3. New N-terminal fluorescent peptide products were detected for five of the 10 substrates (BS-01, -02, -04, -06, and -11) when tested under our experimental conditions, indicating that these substrates were processed by 3CL^{pro}. In all cases, the substrate was cleaved in one position only, consistent with the known specificity of SARS 3CL^{pro} and as expected, since each peptide contained only one glutamine residue (Table 1). Using MALDI-TOF MS analysis, we confirmed that the molecular masses of all the BS-IQFS cleavage products generated by recombinant 3CL^{pro} correspond to that of the expected N-terminal fragments following cleavage after the glutamine residue (data not shown).

Determination of relative cleavage efficiencies of BS-IQFSs by 3CL^{pro} using a continuous fluorescence assay

Having identified which blue-shifted IQFSs were detectably processed by 3CL^{pro} *in vitro*, we then compared their relative cleavage efficiencies in real time using a continuous fluorescence assay. A representative plot showing the fluorescence released from protease assay reactions containing 50 μM of either BS-01, -02, -04, -06, or -11 over a period of 3 h at 30°C is shown in Figure 4. Substrates BS-01, -06, and -11 were all efficiently cleaved, resulting in a substantial increase in fluorescence detected following addition of 3CL^{pro} at time zero. Substrates BS-02 and -04 were considerably less well processed, displaying only a modest increase in the fluorescent signal detected. The average rate of fluorescence emitted per min for each substrate is also plotted in bar chart form (Figure 4, inset), showing that peptide BS-01 was the most efficiently processed substrate. Online monitoring also revealed that for several of the blue-shifted substrates, there was an initial 'lag' period during which there was very little detectable processing. In fact, for substrates BS-02, -04, and -06, a decrease in fluo-

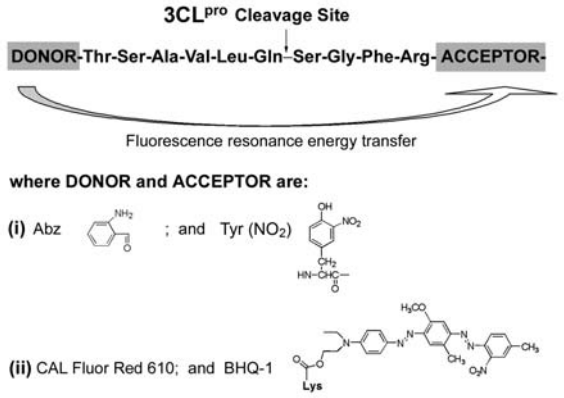

Figure 2 Sequences of SARS-CoV 3CL^{pro} IQFSs.
The amino acid sequences of blue- and red-shifted fluorogenic substrates (i) BS-01 and (ii) RS-01, as well as the chemical structures of the fluorescent donor group *O*-aminobenzoyl (Abz) and quenching moieties 3-nitro-tyrosine [Tyr(3-NO_2)] and Black Hole quencher-1 (BHQ-1) are shown.

rescence was initially observed, presumably a consequence of changes in the assay microenvironment resulting in increased quenching efficiency within these specific peptides. The negative signal is overcome as processing occurs. For inhibitor screening, particularly in high-throughput formats, the substrate used should ideally be processed efficiently to generate a strong signal with no lag period. As it fulfils both these criteria, we selected BS-01 as the optimal blue-shifted substrate for continuous monitoring of 3CL^{pro} activity. We also performed kinetic analysis using BS-01. K_m and k_{cat} values of 146±19 μM and 0.38±0.01 min^{-1}, respectively, were calculated for this substrate.

Determination of the quenching factor for the blue-shifted and red-shifted substrates BS-01 and RS-01 and fluorescence emission spectra

Since BS-01 was the substrate most efficiently cleaved in our continuous assay, we chose this peptide sequence to synthesise a further fluorogenic substrate for 3CL^{pro} using a different fluorescent donor and quencher pair. Substrate RS-01 has a red-shifted fluorophore (CAL Fluor Red 610) combined with the BHQ-1 quencher group (Table 1; Figure 2). We were interested in generating a red-shifted fluorescent peptide substrate, since this may offer a significant advantage over blue-shifted peptides for inhibitor screening using libraries containing natural or synthetic coloured compounds, as the number of false positives resulting from non-specific interference with the fluorophore group may be reduced (Grant et al., 2002; see below). Emission scans for BS-01 (Figure 5A) and RS-01 (Figure 5B) were run in the presence or absence of Pronase E, an endoprotease with broad specificity (see materials and methods). As previously reported (Jean et al., 1995), the fluorescence of the undigested BS-01 (Figure 5A, t=0 min) was expected, since the donor and acceptor [Abz/Y(3-NO_2)] are located at a significant distance from each other (10 amino acids), thus lessening the quenching effect (quenching factor 14±3), as observed in Figure 5A (see also materials and methods). In contrast, the emission scan of the undigested RS-01 revealed very low background fluorescence (Figure 5B, t=0 min). The quenching factor for RS-01 was estimated as 137±7 (Figure 5B; see materials and methods), a value approximately 10-fold greater than that determined for BS-01. Moreover, fluorescence emission spectra of the cleaved fluorescent N-terminal moiety of RS-01 revealed an emission wavelength maxima of ca. 612 nm upon excitation at 584 nm. The results of this study demonstrate that in spite of the distance separating the RS-01 fluorescent donor/acceptor pair, the highly fluorescent CAL Fluor Red 610 is efficiently quenched by long-range resonance energy transfer to the BHQ-1 group at excitation and emission wavelengths of 584 and 612 nm.

Processing of red-shifted IQFSs by 3CL^{pro}

Protease assay reactions containing 30 μM RS-01 were carried out under the same conditions as described for

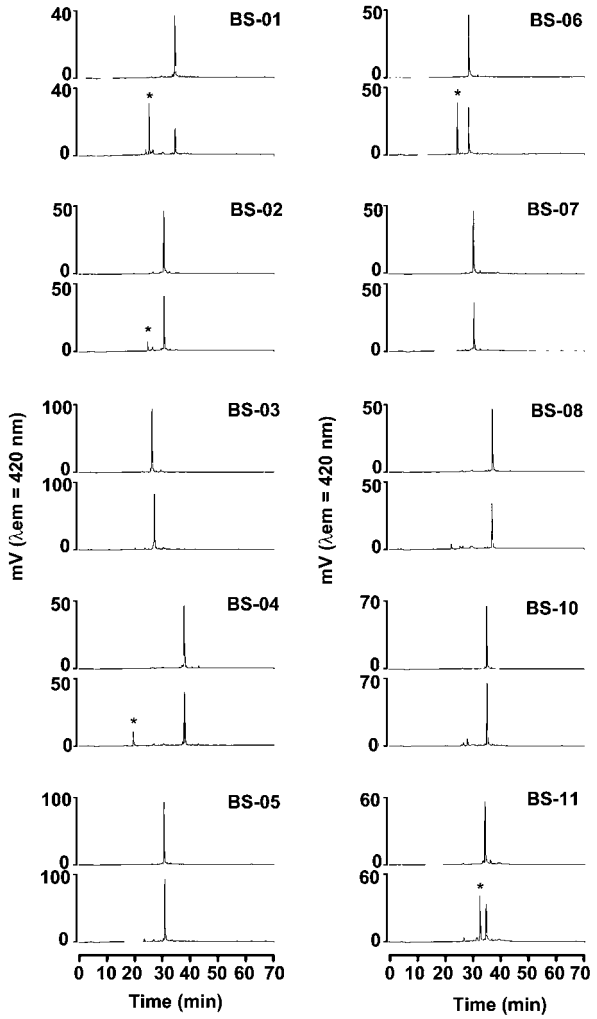

Figure 3 Processing of blue-shifted IQFSs by SARS-CoV 3CL^{pro}.
RP-HPLC chromatograms showing the separation of fluorescent IQFS digestion products produced in protease assays containing blue-shifted IQFS. Peptides were detected using excitation and emission wavelengths of 320 and 420 nm, respectively. For each IQFS, fluorescent peptides present in reactions either in the absence (upper panel) or presence (lower panel) of 3CL^{pro} are shown. Peaks corresponding to cleaved BS-IQFS are indicated with an asterisk.

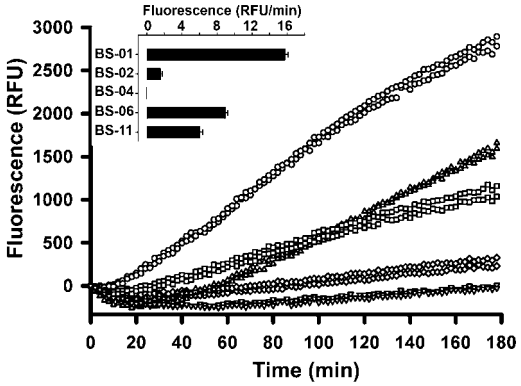

Figure 4 Continuous monitoring of SARS-CoV 3CL^{pro} activity using blue-shifted IQFSs.

The fluorescent signal emitted in real time from protease assay reactions containing 50 μM of either BS-01 (○), BS-02 (◇), BS-04 (▽), BS-06 (△), or BS-11 (□) following addition of 175 nM 3CL^{pro} at time zero is shown. The average rate of increase in fluorescent signal resulting from 3CL^{pro} processing for each blue-shifted substrate is shown in the inset.

blue-shifted substrates and then analysed by RP-HPLC using a fluorescence detector to determine whether this substrate is processed by recombinant 3CL^{pro} *in vitro* (materials and methods). Representative chromatograms showing the resolution of fluorescent peptide species in reactions containing RS-01 either in the presence or absence of 3CL^{pro} are shown in Figure 6A. As expected, analysis of assay reactions containing 30 μM RS-01 without 3CL^{pro} revealed that the CAL Fluor Red 610 fluorophore is very efficiently quenched by the BHQ-1 group in the intact peptide, since it is barely detectable by fluorescence monitoring (Figure 6A, panel 2). In fact, we only detected the intact peptide when injected at concentrations considerably higher than those used in protease assay reactions, such as 200 μM (59 min; Figure 6A, panel 1), again indicative of a high quenching factor for RS-01 (Figure 5B). The presence of a novel fluorescent product within assay reactions containing 3CL^{pro} confirms that RS-01 is processed and, as expected, that cleavage occurs at one position only (44 min; Figure 6A, panel 3). This product shares the same retention time as that of the RS-01 STD^{Nt} peptide (CAL Fluor Red 610-TSAVLQ-OH), which is eluted at 44 min (Figure 6A, panel 4), confirming that it corresponds to the expected N-terminal fragment following cleavage after the glutamine residue. We then assessed whether RS-01 was suitable for continuous monitoring of 3CL^{pro} protease activity under the same conditions as described for the blue-shifted substrates. Figure 6B shows a representative plot of fluorescence detected in real time from reactions containing 30 μM RS-01 in the presence or absence of 3CL^{pro}. RS-01 is processed very efficiently, resulting in a rapid increase in fluorescence detected following addition of 3CL^{pro} at time zero, with no lag period. On-line monitoring also showed that the baseline fluorescence signal in the absence of protease is stable (Figure 6B).

Determination of kinetic parameters for 3CL^{pro} using red-shifted IQFS

Having established that RS-01 is a sensitive substrate for continuous monitoring of 3CL^{pro} activity, we sought to determine the kinetic parameters of 3CL^{pro} using this substrate. Protease assays were performed in the presence of a range of concentrations of RS-01 (7.5–50 μM). Initial velocity values were then fitted to the Michaelis-Menten rate equation (Enzyme Kinetics module, SigmaPlot) to determine K_m and estimate the k_{cat} values, which were found to be 14±2 μM and 0.65±0.01 min^{-1}, respectively (values represent the average of two independent experiments carried out in duplicate). A representative plot is shown in Figure 6C. This K_m value is comparable to others previously reported that used fluorogenic peptide substrates also derived from the SARS polyprotein nsp4/nsp5 junction (Kuo et al., 2004; Liu et al., 2005).

Use of the continuous fluorescence assay using red-shifted IQFS to identify a novel small-molecule inhibitor of SARS-CoV 3CL^{pro}

We then sought to apply our novel continuous assay using RS-01 to screen compound libraries to identify inhibitors of 3CL^{pro} activity. Assays were carried out as previously described with the exception that 3CL^{pro} and test compounds were pre-incubated for 15 min at 30°C before reactions were initiated by addition of RS-01. Initially, we screened extracts from marine organisms, which led to the identification of a novel inhibitor of recombinant 3CL^{pro} *in vitro.* The active component, escu-

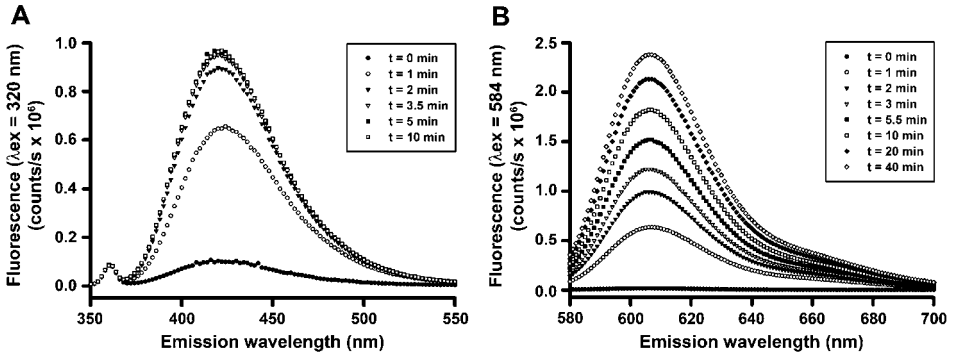

Figure 5 Fluorescence emission spectra of undigested IQFSs and fluorescent products of digestion of IQFSs by Pronase E.

Emission spectra for uncleaved (t=0 min) and cleaved (t>0 min) BS-01 (A) and RS-01 (B) substrates. Conditions are described in materials and methods. Legends in (A) and (B) indicate the time (min) of each enzymatic reaction.

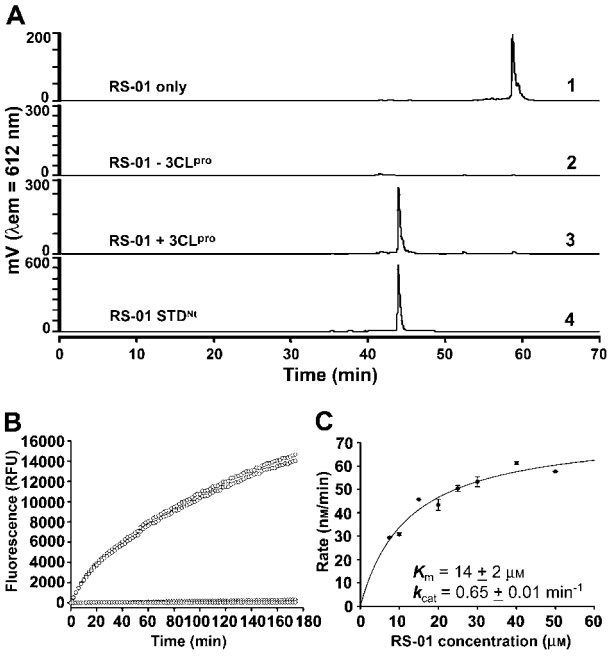

Figure 6 Validation of red-shifted IQFS for continuous monitoring of 3CL^{pro} activity and detection of inhibitors.
(A) RP-HPLC analysis showing processing of RS-01 substrate by 3CL^{pro}. Representative chromatograms demonstrating the separation of fluorescent peptides contained in protease assay reactions containing 30 μM RS-01 substrate in the absence or presence of 117 nM 3CL^{pro} are shown (panels 2 and 3), as well as chromatograms indicating the retention time of intact RS-01 (200 μM) (panel 1) or RS-01 STD^{Nt} (CAL Fluor Red 610-TSAVLQ-OH, panel 4). (B) Continuous monitoring of 3CL^{pro} activity using RS-01. The fluorescent signal emitted in real time from assay reactions containing 30 μM RS-01 in the presence (○) or absence (◇) of 117 nM 3CL^{pro}. (C) Kinetic parameters obtained using RS-01. The initial velocity of 3CL^{pro} in reactions containing RS-01 in the concentration range 7.5–50 μM is shown.

letin-4-carboxylic acid ethyl ester (MC8), has been identified as a coumarin derivative previously isolated from the marine sponge *Axinella corrugata* (M.H.R. Seleghim, S.P. de Lira, D.E. Williams, F. Marion, P. Hamill, F. Jean, R.J. Andersen, R.G.S. Berlinck and E. Hajdu, unpublished results).

Pre-incubation with MC8 led to a decrease in the fluorescence signal detected for assay reactions containing 3CL^{pro} and RS-01 in a dose-dependent manner within the range of concentrations tested (40–800 μM), as shown in Figure 7A. The residual activity of 3CL^{pro} pre-incubated with MC8 was then plotted as a function of the inhibitor concentration (log scale) to determine the median inhibitory concentration (IC_{50}) for this novel inhibitor (Figure 7B). The residual activity of 3CL^{pro} in the presence of a known small-molecule inhibitor, MP576, was also plotted as a positive control. MP576 is a reversible inhibitor of recombinant 3CL^{pro} activity that also exhibits anti-SARS-CoV activity in Vero cells (Kao et al., 2004a,b). The IC_{50} values for MC8 and MP576 were found to be 46±7 and 45±1 μM, respectively (Figure 7B). Protease assay reactions were also analysed by RP-HPLC to confirm that the inhibition observed was not due to non-specific interference of the coloured MC8 compound with the CAL Fluor Red 610 fluorophore. Chromatograms showing the resolution of fluorescent peptides within assay reactions containing 3CL^{pro} and 30 μM RS-01 in the absence or presence of 800 μM MC8 are shown in Figure 7C. A chromatogram indicating the retention time of cleaved RS-01 is also shown (50 μM RS-01 STD^{Nt} peptide; 44 min, Figure 7C). This peak is present in samples without MC8, but absent in the sample in which 3CL^{pro} and MC8 were pre-incubated, confirming that processing of RS-01 is completely inhibited in the presence of 800 μM MC8.

Interestingly, when MC8 was pre-incubated with BS-01 (30 μM) and RS-01 (30 μM) in the absence of SARS-CoV 3CL^{pro} (materials and methods), we observed that the coloured compound caused high levels of interference only when tested with the BS-01 substrate (Figure 8). The BS-01 fluorescence signal obtained in the presence of 200 μM MC8 was dramatically decreased by 39±2% (Figure 8; signal 741±27 for + MC8, 1210±9 for the control). In contrast, RS-01 fluorescence signals in the presence of 200 μM MC8 were not significantly dif-

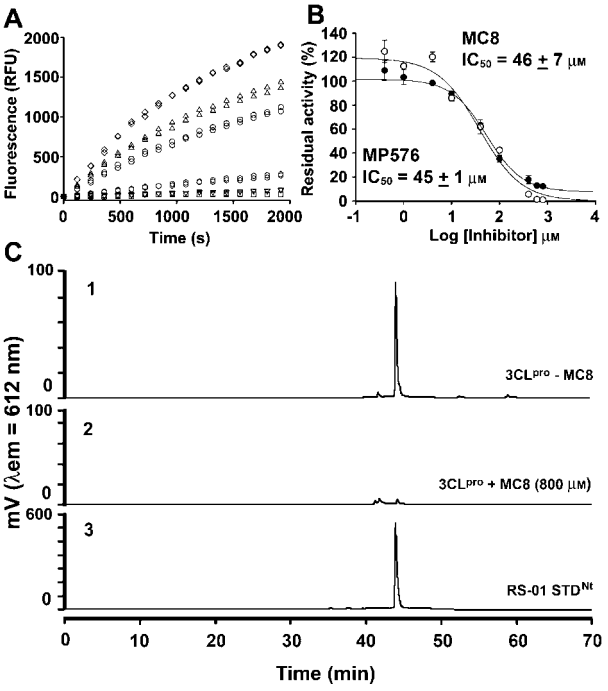

Figure 7 Identification of a novel 3CL^{pro} inhibitor by screening a library of naturally occurring marine compounds.
(A) Compound MC8 inhibits 3CL^{pro} activity in a dose-dependent manner. 3CL^{pro} (117 nM) was pre-incubated with or without MC8 for 15 min at 30°C, then protease assay reactions were started by the addition of 30 μM RS-01. The fluorescence detected from duplicate protease reactions containing no MC8 (◇), 40 μM (△), 100 μM (○), 400 μM (○), or 800 μM (▽) MC8 is plotted against time (□, RS-01 only). (B) Determination of the IC_{50} value for MC8 and comparison with the known inhibitor MP576. The residual activity of 3CL^{pro} pre-incubated with MC8 or MP576 at the concentrations indicated was plotted as a percentage of 3CL^{pro} activity in the absence of inhibitor to derive IC_{50} values using curve-fitting (○ MC8; ● MP576). (C) RP-HPLC analysis demonstrating the inhibition of 3CL^{pro} activity by MC8. Representative chromatograms showing the separation of fluorescent peptides contained in protease assay reactions containing 30 μM RS-01 substrate in (1) the absence or (2) presence of 800 μM MC8 and (3) indicating the retention time of RS-01 STD^{Nt} (CAL Fluor Red 610-TSAVLQ-OH).

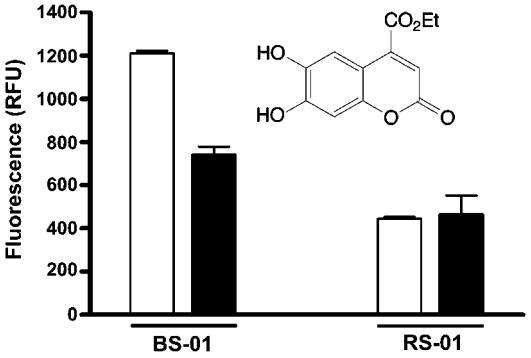

Figure 8 MC8 causes high levels of interference for fluorescence measurements performed using BS-01, but not RS-01.
BS-01 (30 μM) and RS-01 (30 μM) were incubated in the absence (open bars) or presence (filled bars) of MC8 (200 μM) in SARS-CoV 3CL^{pro} assay buffer in a total volume of 100 μl in 96-well plates for 1 h at 30°C. The fluorescence signal was monitored using a SpectraMax Gemini XS spectrofluorimeter with excitation and emission wavelengths of 320 and 420 nm (BS-01) or 584 and 612 nm (RS-01), respectively (see materials and methods). Fluorescence data associated solely with each fluorophore were obtained by subtracting the relative fluorescence unit measured in wells containing only the assay buffer from the fluorescence signal obtained for each reaction performed with IQFS, or IQFS and MC8. Experiments were carried out in quadruplicate. The bar chart represents the average of two separate experiments. The mean value is shown with SD. The inset shows the chemical structure of MC8.

ferent (Figure 8; 465±61 for +MC8, 444±6 for the control). The results of this experiment clearly demonstrate that in contrast to the red-shifted fluorophore Cal Red 610, the blue-shifted fluorophore Abz is readily susceptible to interference/quenching by coloured natural compounds such as MC8.

Inhibition of SARS-CoV replication in Vero cells by MC8

Having established that MC8 effectively inhibits recombinant 3CL^{pro} activity *in vitro*, we then investigated whether it displays any anti-viral properties in cell-based assays of SARS-CoV infection. Vero cells are permissive to SARS-CoV infection and are routinely used to propagate the virus. Infection of these cells by SARS-CoV causes a significant cytopathic effect (CPE). Hence, they are especially useful for quickly assessing the anti-viral effects of test compounds, because inhibition of viral replication causes a corresponding reduction in the CPE observed. Vero cell monolayers were infected with SARS-CoV strain HKU39849 in the presence or absence of MC8 (Figure 9A–E). The extent of CPE in cell monolayers was then assessed 48 h post-infection. Representative images of Vero cell monolayers are shown in Figure 9. Figure 9A shows uninfected cells, with the monolayer intact, as expected. In contrast, cells infected with SARS-CoV exhibited significant CPE (Figure 9B). However, very little CPE was observed in infected cells treated with 50 μM MC8, indicating that this compound protects against SARS-CoV-induced CPE (Figure 9C). Uninfected cells treated with 50 μM MC8 appear identical to uninfected cells without MC8, indicating that MC8 doses effective at preventing CPE do not cause observable toxic effects (Figure 9D).

To further assess the anti-SARS-CoV properties of MC8, we performed virus plaque reduction assays in Vero cells. Monolayers of Vero cells were infected with SARS-CoV strain HKU39849 in the presence (25–400 μM) or absence of MC8. The number of plaque-forming units (PFU) was counted after 48 h and then plot-

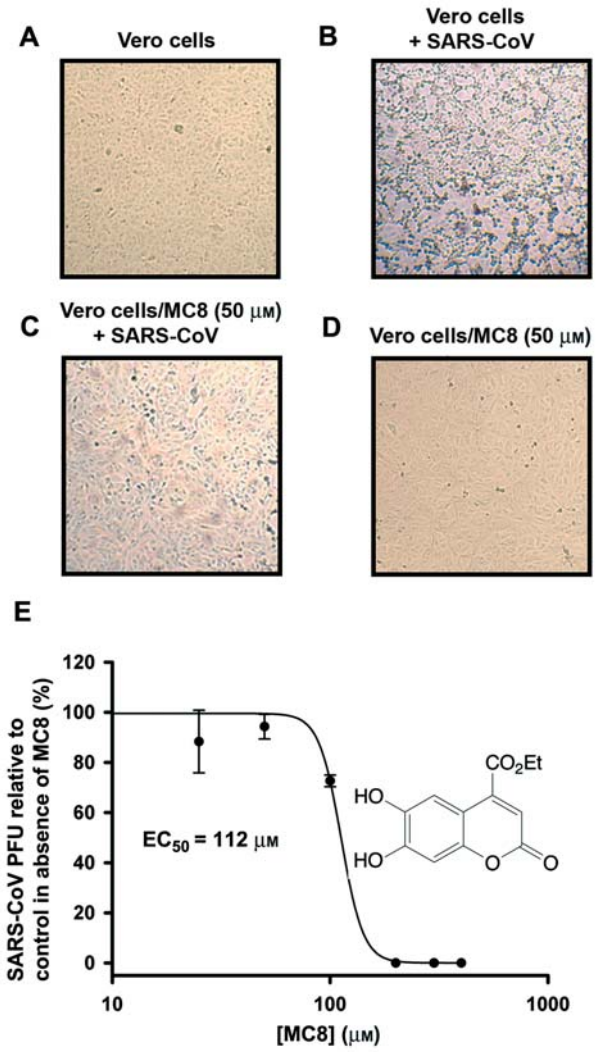

Figure 9 Inhibition of SARS-CoV replication in Vero cells by MC8.
(A–D) MC8 protects Vero cells from SARS-CoV-induced CPE. Vero cell monolayers were infected with 100 $TCID_{50}$ of SARS-CoV HKU39849 or mock-infected either in the presence or absence of 50 μM MC8. After 48-h incubation, cells were photographed using a digital imaging system in conjunction with a Leica DMIL inverted microscope. Representative images of (A) uninfected cells, (B) SARS-CoV-infected cells, (C) SARS-CoV-infected cells in the presence of MC8, and (D) uninfected cells in the presence of MC8. (E) MC8 causes a reduction in SARS-CoV titre in a dose-dependent manner. Monolayers of Vero cells were infected with 100 PFU of SARS-CoV HKU39849 or mock-infected either in the presence or absence of MC8 in the concentration range 25–400 μM. After 2 h, cells were covered with agar overlay and incubated for a further 48 h. Cells were then fixed and stained using crystal violet so that viral plaques could be counted. The number of PFUs was then plotted as a function of MC8 concentration, and the data were fitted using SigmaPlot 8.0 to derive the EC_{50} value, which was found to be 112 μM.

ted as a function of MC8 concentration to obtain the EC_{50} value for MC8 in the cell culture. EC_{50} (median effective concentration) was determined by fitting the data to a best-fit equation (Figure 9E). An EC_{50} value of 112 μM was determined for inhibition of viral replication by MC8 in Vero cells. This represents only approximately a three-fold difference from the IC_{50} value obtained for inhibition of recombinant $3CL^{pro}$ activity *in vitro* (46 μM). This may be explained by reduced accessibility of the protease to MC8, since the inhibitor has to permeate the cell membrane. These data indicate that MC8 is a promising inhibitor of SARS-CoV replication, especially considering that the TC_{50} (median toxic concentration) of MC8 is higher than 800 μM (the highest concentration of MC8 tested), as determined by MTT assay (data not shown).

Discussion

We have described a continuous *in vitro* FRET-based assay system for monitoring SARS-CoV $3CL^{pro}$ enzyme activity using novel blue- and red-shifted fluorogenic peptide substrates, which we applied to identify a novel $3CL^{pro}$ inhibitor compound, MC8, derived from the marine sponge *Axinella corrugata*.

Our assay is performed in a format suitable for high-throughput screening. Since it monitors $3CL^{pro}$ activity in real time, it allows information regarding both the efficacy and mode of action of novel inhibitors to be gathered. While developing our assay, we generated a series of blue- and red-shifted fluorogenic peptides to identify an optimal substrate for kinetic analysis and to screen compound libraries to identify novel $3CL^{pro}$ inhibitors. Both BS-01 and RS-01 substrates proved to be useful for continuous monitoring of $3CL^{pro}$ activity and for kinetic analysis. K_m and k_{cat} values of 146±19 μM and 0.38± 0.01 min^{-1}, respectively, were obtained for the BS-01 substrate, which are consistent with values obtained for other blue-shifted substrates of the same length based on SARS polyprotein cleavage junctions (Kuang et al., 2005).

Several studies have already successfully used blue-shifted substrates to monitor $3CL^{pro}$ activity and to screen for novel inhibitors (Liang, 2006). However, it is increasingly recognised that there are limitations to the use of blue-shifted fluorophores in FRET-based assays for screening small compound libraries, owing to non-specific interference between naturally coloured compounds and fluorophores with emission maxima within the blue or ultraviolet part of the spectrum. Non-specific interference increases the amount of false positive hits, which can hinder progress in high-throughput screening efforts. One strategy to reduce the level of interference by test compounds in FRET-based assays is to use red-shifted fluorophores with longer-wavelength characteristics (Grant et al., 2002; George et al., 2003), since there is generally less non-specific interference from organic compounds with fluorophores from within the red region of the spectrum. Red-shifted peptide substrates may therefore offer a significant advantage over blue-shifted peptides for inhibitor screening. Hence, we synthesised a novel peptide substrate containing a red-shifted fluorescent donor. Substrate RS-01 is characterised by a novel fluorescent donor/acceptor pair: Cal Red 610 and BHQ-1. To the best of our knowledge, this is the first time that this pair has been used together in a fluorogenic peptide substrate, although BHQ-1 has been successfully used as a quenching moiety in DNA oligonucleotide applications (Wilson and Johansson, 2003; Boguszewska-Chachulska et al., 2004; Johansson et al., 2004; Moreira et al., 2005).

The intramolecular quenching efficiency in RS-01 was found to be extremely efficient (quenching factor >100) when compared to the value determined for BS-01 (quenching factor >10). In addition, in contrast to some of the blue-shifted substrates tested, the baseline fluorescent signal in the absence of protease is very stable. Kinetic analysis using RS-01 revealed that it is a sensitive substrate that is efficiently processed by $3CL^{pro}$ to produce a strong increase in fluorescence with no lag period. K_m and k_{cat} values of 14±2 μM and 0.65±0.01 min^{-1}, respectively, were obtained for RS-01, with an overall performance constant (k_{cat}/K_m) that was 20-fold better than for BS-01 (52.8 vs. 2.6 min^{-1} mM^{-1}). Hence, RS-01 possesses several important biophysical properties that make it well suited for continuous monitoring of $3CL^{pro}$ activity and high-throughput screening (HTS) applications. Moreover, the donor/acceptor pair developed in this study is of great interest for the design and development of novel red-shifted IQFSs for HTS directed at other important virally encoded proteases, such as hepatitis C virus (HCV) non-structural (NS)3-NS4A heterocomplex protease, a prime target for anti-HCV therapies (Richer et al., 2004; Hamill and Jean, 2005).

We used our assay to begin screening a library of naturally occurring compounds derived from marine organisms. The marine environment is recognised as being an extremely rich source of chemically diverse metabolites with numerous potential pharmaceutical applications. Many natural products from marine organisms are currently under investigation for cancer and pain treatments (Newman and Cragg, 2004), but they are also of interest for their potential as novel anti-viral therapies (Gustafson et al., 2004). Numerous compounds derived from marine organisms have been shown to exhibit anti-HIV activity through targeting a variety of essential HIV-specific enzymes, including the viral protease (Patil et al., 1992). Hence, it was of interest to us to screen our marine extracts for SARS-CoV $3CL^{pro}$ inhibitory activity.

Since the majority of these compound mixtures are coloured, we utilised our red-shifted substrate to evaluate the test compounds. An initial screen using BS-01 indicated that approximately 50% of the marine extracts tested were $3CL^{pro}$ inhibitors; however, the majority of these were found to be false positives by RP-HPLC analysis (data not shown). However, using the RS-01 substrate, we identified a novel inhibitor of $3CL^{pro}$ activity within the ethanol-soluble fraction of a marine extract. The inhibitory compound was identified as esculatin-4-carboxylic acid ethyl ester (MC8), a novel coumarin derivative extracted from the tropical marine sponge *Axinella corrugata*. The structure of MC8 and a protocol for its

synthesis have been established by Seleghim and collaborators (M.H.R. Seleghim, S.P. de Lira, D.E. Williams, F. Marion, P. Hamill, F. Jean, R.J. Andersen, R.G.S. Berlinck and E. Hajdu, unpublished results). On-line monitoring showed a reduction in processing of red-shifted substrate RS-01 in samples in which 3CL^{pro} was pre-incubated with MC8 in a dose-dependent manner. The inhibitory activity of MC8 was also confirmed by RP-HPLC analysis. An IC_{50} value of 46 μM was determined for MC8 inhibition of recombinant 3CL^{pro} *in vitro*. Moreover, our study demonstrated that in contrast to the widely used blue-shifted donor/acceptor pair [Abz/Y(3-NO_2)] (Liang, 2006), our novel red-shifted donor/acceptor pair (Cal Fluor Red 610/BHQ-1) is not susceptible to interference/quenching by natural coloured compounds such as MC8.

We then assessed whether MC8 displays anti-SARS-CoV activity using tissue culture-based assays in Vero cells. Since SARS-CoV 3CL^{pro} is considered essential for viral replication, we anticipated that inhibition of 3CL^{pro} activity in infected cells would result in a decrease in the viral titre generated and a concomitant reduction in the extent of CPE observed. Treatment of cells with 25–400 μM MC8 prior to infection with SARS-CoV was found to protect against CPE and caused a reduction in the amount of progeny virus produced in infected Vero cells, as determined by a plaque reduction assay, presumably through inhibition of 3CL^{pro} activity in infected cells. Thus, using tissue culture assays, we showed that MC8 is cell-membrane permeable and, importantly, that its effects on SARS-CoV replication are mediated at concentrations that are non-cytotoxic (EC_{50}=112 μM). Our studies so far indicate that the inhibitory activity of MC8 is specific for the viral protease, since no toxic effect was observed in Vero cells treated with concentrations up to 800 μM (TC_{50}>800 μM). Since the structure of MC8 has already been solved, this may serve as a useful starting point for the rational design of analogues with improved 3CL^{pro} inhibitory properties.

Importantly, the results of our work also underline the importance of screening chemically diverse metabolite libraries obtained from marine sponges for the discovery of novel protease inhibitors with potent antiviral activities and a good therapeutic index.

Materials and methods

Synthesis of internally quenched fluorogenic peptide substrates (IQFSs)

Blue-shifted IQFSs BS-01 to BS-11 (Table 1) were synthesised by solid-phase synthesis with the Fmoc [*N*-(9-fluorenyl) methoxycarbonyl] methodology using a multiple automated peptide synthesiser and purified using RP-HPLC as previously described (Jean et al., 1995; Richer et al., 2004; Hamill and Jean, 2005). Red-shifted IQFS RS-01 and CAL Fluor Red 610 standard peptide (RS-01 STD^{Nt}) were synthesised as previously described (Carter et al., 2004). In all cases, peptide purity and composition were demonstrated by RP-HPLC, matrix-assisted laser desorption ionisation time-of-flight (MALDI-TOF) or electrospray mass spectrometry, and amino-acid analysis [University of Toronto, Advanced Protein Technology Centre (APTC), Toronto, Canada] respectively. Stock peptide solutions, quantified by amino-acid analysis (APTC), were prepared in 10 mM DMSO and stored at -20°C.

Expression and purification of His-tagged SARS-CoV 3CL protease (3CL^{pro})

The expression and purification of SARS-CoV 3CL^{pro} has been described previously (Blanchard et al., 2004). All purification steps were carried out at 4°C. The bacterial expression plasmid for SARS-CoV TOR2 strain 3CL^{pro} was kindly provided by Dr. Lindsay Eltis (Department of Microbiology, University of British Columbia). Briefly, recombinant SARS-CoV 3CL^{pro} was expressed in the cytosol of bacteria (*E. coli* BL21 pLysS) and purified from clarified bacterial cell lysate by nickel-binding interaction chromatography (HiTrap Columns; GE Healthcare/Amersham Biosciences, Baie d'Urfé Quebec, Canada) using an AKTApurifier FPLC system (GE Healthcare/Amersham Biosciences), except plasmid pT7HSP2 was transformed into *E. coli* BL21 strain (Novagen, San Diego, CA, USA). Cultures were grown at 37°C in LB medium containing 100 μg/ml ampicillin. Upon reaching A_{600}=0.6, cells were induced to express 3CL^{pro} by addition of 1 mM isopropyl-1-thio-β-D-galactopyranoside at 37°C for 3 h. Pelleted cells were lysed in buffer A (Fan et al., 2004; 40 mM Tris-HCl, pH 8.0, 100 mM NaCl, 10 mM imidazole, 7.5 mM 2-mercaptoethanol) by sonication. Cell lysates were clarified by centrifugation at 24 *g* for 20 min at 4°C. Then the soluble fraction was applied to a 1-ml HiTrap HP Ni^{2+} chelating column (GE Healthcare/Amersham Biosciences) previously equilibrated with 50 ml of buffer A at a flow rate of 1 ml/min. The loaded column was then washed using 100 ml of buffer A. Bound proteins were eluted using a 1–100% gradient of buffer B (40 mM Tris-HCl, pH 8.0, 100 mM NaCl, 250 mM imidazole, 7.5 mM 2-mercaptoethanol). Fractions containing His-tagged 3CL^{pro} were pooled and dialysed (Slide-a-lyzer, 3.5-kDa cutoff; Pierce, Rockford, IL, USA) for three 1-h periods at 4°C in buffer C (50 mM Hepes, pH 7.3, 100 mM NaCl, 7.5 mM 2-mercaptoethanol). Proteins were aliquoted, snap-frozen, and stored at -86°C. Protein purity and composition for 3CL^{pro} were demonstrated by Coomassie blue staining (Figure 1) and amino acid analysis (APTC).

Enzyme assays

SARS-CoV 3CL^{pro} assay reactions in a total volume of 100 μl in 96-well plates were performed with a protease assay buffer consisting of 50 mM Hepes, pH 7.3, 100 mM NaCl, 10 mM dithiothreitol, and 10 μg/well bovine serum albumin (BSA). 3CL^{pro} was added to reactions at concentrations within the range 117–175 nM. Reactions were started by the addition of fluorogenic substrate at the concentrations indicated. Protease activity was monitored using a SpectraMax Gemini XS spectrofluorimeter equipped with a temperature-controlled 96-well plate reader, set at excitation and emission wavelengths of either 320 and 420 nm for blue-shifted substrates or 584 and 612 nm for red-shifted substrates, respectively. The initial rate of cleavage (v_i) was determined using the data recorded for each reaction from the linear positive slope of the progress curve (<10% substrate conversion) after addition of the IQFS. To confirm the scissile bond cleaved by recombinant 3CL^{pro}, reactions were stopped by the addition of 0.3% formic acid and then analysed by MALDI-TOF MS or electrospray MS (Genome BC Proteomics Centre, Victoria, BC, Canada).

Inhibitor assays

Protease assay reactions containing 3CL^{pro} and either MP576 or MC8 as inhibitor were pre-incubated for 15 min at 30°C. Reac-

tions were started by the addition of substrate and performed as described above.

Determination of kinetic parameters: K_m, V_{max} and k_{cat}

The kinetic parameters K_m (Michaelis-Menten constant) and V_{max} (maximal velocity) were obtained from non-linear least-squares fit of initial velocity data to the hyperbolic Michaelis-Menten rate equation using SigmaPlot 2000 Enzyme Kinetic Module 1.0 (Systat Software, Inc., Point Richmond, CA, USA). The amount of cleaved IQFS product generated was determined by extrapolation of values from a standard curve of fluorescence vs. concentration for Abz-peptidyl-OH and CAL Fluor Red 610-peptide-OH standards. The turnover number (k_{cat}) was calculated from V_{max}/E_T, where E_T was determined by amino acid analysis (APTC). Therefore, in this study the k_{cat} values reported are based on the assumption that all the SARS-CoV molecules quantified by amino acid analysis are enzymatically active.

Reversed-phase HPLC

Protease assay reactions were resolved by RP-HPLC on a Vydac monomeric C18 column using a Polaris 212 system equipped with a model 363 fluorescence detector (Varian Inc., Mississauga, Ontario, Canada). Samples were resolved using a linear gradient of 5–70% acetonitrile/0.1% CF_3COOH over 65 min (1 ml/min). Eluted proteins were detected by UV absorbance at 225 nm and fluorescent IQFS cleavage products were detected using excitation and emission wavelengths of 320 and 420 nm for BS-IQFS or 584 and 612 nm for RS-IQFS, respectively.

Fluorescence emission spectra of uncleaved and cleaved IQFSs and determination of quenching factors

Emission scans were run in 3-ml volumes in quartz cuvettes on a Model 814 spectrofluorimeter (Photon Technologies International, London, Ontario, Canada) using an excitation wavelength of 320 or 584 nm to measure the fluorescence signal of the blue-shifted fluorophore (Abz) or red-shifted fluorophore (CALFluorRed610), respectively. The fluorescence emission spectra of uncleaved IQFSs were obtained in assay buffer consisting of 50 mM Tris-HCl (pH 7.9) and BS-01 (1.15 μM) or RS-01 (0.36 μM) in the absence of protease. The reactions were started with Pronase E (Sigma, St. Louis, MO, USA; P6911; EC 232-909-5), an endoprotease with broad specificity. Emission scans of the blue-shifted (350–550 nm, 2-nm bandwidth) and red-shifted (580–700 nm, 2-nm bandwidth) cleaved fluorescent N-terminal moiety were recorded at various time intervals for up to 40 min at 30°C (Figure 5). Initially, 82 nM Pronase E was used for digestion of each IQFS. Later, complete digestion of BS-01 and RS-01 substrates was carried out by 10-min incubation with 8.2 nM Pronase E and 40-min incubation with 82 nM Pronase E, respectively (Figure 5).

The quenching factors for BS-01 and RS-01 were determined as previously described (Jean et al., 1995). Briefly, assay reactions in a total volume of 150 μl were performed in 96-well plates with protease assay buffer consisting of 50 mM Tris-HCl (pH 7.9) and either BS-01 (3.0 and 30 μM) or RS-01 (2 and 20 μM). The IQFSs were incubated for 1 h at 30°C in the absence or presence of Pronase E (295 nM). The relative fluorescence units (RFU) of the reactions performed in the absence (uncleaved IQFS, RFU_{uncl}) or presence of the protease (cleaved IQFS, RFU_{cl}) were determined using a Safire spectrofluorimeter (Tecan, Männedorf, Switzerland) set at excitation and emission wavelengths of either 320 and 420 nm (BS-01) or 584 and 612 nm (RS-01). The quenching factor corresponds to the ratio RFU_{cl}/RFU_{uncl} (Jean et al., 1995).

Virus plaque reduction assay

Tissue culture plates (24-well; TPP, Trasadingen, Switzerland) with a confluent monolayer of Vero cells (1×10^5 cells/well) grown in complete Eagle minimal essential medium (EMEM; Invitrogen, Grand Island, USA) with 1% foetal bovine serum (FBS; Invitrogen) were prepared. Then 100 PFU of SARS-CoV strain HKU39849 was added to each well with or without the addition of MC8. After incubation for 2 h at 37°C with 5% CO_2, the cell culture media and unbound viral particles were aspirated and 1 ml of overlay (1% low-melting agarose in EMEM with 1% FBS and appropriate concentrations of inhibitors) was immediately added to each well. Plates were further incubated for 48 h under identical conditions. Cells were fixed by adding 1 ml of 10% formaldehyde. The agarose plugs were then removed and the cells were stained with 0.5% crystal violet in 70% methanol and the viral plaques were counted. Experiments were carried out in triplicate and repeated twice. Values are reported as mean with SD. Dose-response data were fitted to a logistic equation (SigmaPlot 8.0; Systat). PFU was plotted as a percentage relative to PFU generated in the absence of inhibitor.

SARS-CoV CPE assay

Vero cells were seeded at 2×10^4 cells/well in complete EMEM supplemented with 5% heat-inactivated FBS, with or without the addition of MC8. Then 100 $TCID_{50}$ (50% tissue-culture infectious dose) of SARS-CoV strain HKU39849 was added to each well. Assay plates were incubated at 37°C in 5% CO_2 for 48 h. The CPE of infected cells was photographed using a Leica DMIL inverted microscope equipped with a DC300F digital imaging system (Leica Microsystems, Wetzlar, Germany).

Cytotoxicity assay

The cytotoxicity of selected compounds was determined by MTT (3-[4,5-dimethylth-iazol-2-yl]-2,5-diphenyltetrazolium bromide) assay (Roche, Mannheim, Germany) according to the manufacturer's instructions. The TC_{50} (median toxic concentration) of MC8 is greater than 800 μM, which was the highest concentration of MC8 tested (in 1% DMSO, v/v).

Acknowledgements

We would like to thank Drs. Raymond J. Andersen and Frederic Marion (Department of Chemistry, University of British Columbia, Canada) for synthesis of the MC8 compound and their collaboration on this project. We are also very grateful to Dr. Wayne Tsuifor (Department of Microbiology, University of Hong Kong, China) for his technical expertise with the SARS-CoV cell culture assays, and we would like to thank Drs. Lindsay Eltis and Pascal Fortin (Department of Microbiology and Immunology, University of British Columbia, Canada) for providing the $3CL^{pro}$ bacterial expression plasmid. Rafael Arze is thanked for synthesis of RS peptides, and Gabriel Martinez for management of spectroscopic data. This work was supported by grants from the Canadian Institutes of Health Research (CIHR)/R&D (DOS-75167) and NCE/PENCE Inc. (G119120086) (to F. Jean), and the Vice-Chancellor SARS Fund and HKU seed grant for basic research (to R.Y. Kao). F. Jean is a CIHR/Health Canada Research Initiative on Hepatitis C Scholar.

References

Anand, K., Palm, G.J., Mesters, J.R., Siddell, S.G., Ziebuhr, J., and Hilgenfeld, R. (2002). Structure of coronavirus main proteinase reveals combination of a chymotrypsin fold with an extra α-helical domain. EMBO J. *21*, 3213–3224.

Anand, K., Ziebuhr, J., Wadhwani, P., Mesters, J.R., and Hilgenfeld, R. (2003). Coronavirus main proteinase (3CLpro) structure: basis for design of anti-SARS drugs. Science *300*, 1763–1767.

Blanchard, J.E., Elowe, N.H., Huitema, C., Fortin, P.D., Cechetto, J.D., Eltis, L.D., and Brown, E.D. (2004). High-throughput screening identifies inhibitors of the SARS coronavirus main proteinase. Chem. Biol. *11*, 1445–1453.

Boguszewska-Chachulska, A.M., Krawczyk, M., Stankiewicz, A., Gozdek, A., Haenni, A.L., and Strokovskaya, L. (2004). Direct fluorometric measurement of hepatitis C virus helicase activity. FEBS Lett. *567*, 253–258.

Carter, T.G., Cook, R.M., Hudson, D., Johansson, M.K., Lyttle, M.H., Reddington, M., and Walton, T. (2004). The synthesis and properties of novel profluorescent peptides containing Black Hole Quenchers™. In: Solid Phase Synthesis and Combinatorial Libraries, R. Epton, ed. (Kingswinford, UK: Mayflower Scientific), p. 103.

Chen, H., Wei, P., Huang, C., Tan, L., Liu, Y., and Lai, L. (2006) Only one protomer is active in the dimer of SARS 3C-like proteinase. J. Biol. Chem. *281*, 13894–13898

Drosten, C., Gunther, S., Preiser, W., van der Werf, S., Brodt, H.R., Becker, S., Rabenau, H., Panning, M., Kolesnikova, L., Fouchier, R.A., et al. (2003). Identification of a novel coronavirus in patients with severe acute respiratory syndrome. N. Engl. J. Med. *348*, 1967–1976.

Fan, K., Wei, P., Feng, Q., Chen, S., Huang, C., Ma, L., Lai, B., Pei, J., Liu, Y., Chen, J., and Lai, L. (2004). Biosynthesis, purification, and substrate specificity of severe acute respiratory syndrome coronavirus 3C-like proteinase. J. Biol. Chem. *279*, 1637–1642.

Fan, K., Ma, L., Han, X., Liang, H., Wei, P., Liu, Y., and Lai, L. (2005) The substrate specificity of SARS coronavirus 3C-like proteinase. Biochem. Biophys. Res. Commun. *329*, 934–40.

George, J., Teear, M.L., Norey, C.G., and Burns, D.D. (2003). Evaluation of an imaging platform during the development of a FRET protease assay. J. Biomol. Screen. *8*, 72–80.

Grant, S.K., Sklar, J.G., and Cummings, R.T. (2002). Development of novel assays for proteolytic enzymes using rhodamine-based fluorogenic substrates. J. Biomol. Screen. *7*, 531–540.

Gustafson, K.R., Oku, N., and Milanowski, D.J. (2004). Antiviral marine natural products. Curr. Med. Chem. Anti-Infect. Agents *3*, 233–249.

Hamill, P. and Jean, F. (2005). Enzymatic characterization of membrane-associated hepatitis C virus NS3-4A heterocomplex serine protease activity expressed in human cells. Biochemistry *44*, 6586–6596.

Jean, F., Basak, A., DiMaio, J., Seidah, N.G., and Lazure, C. (1995). An internally quenched fluorogenic substrate of prohormone convertase 1 and furin leads to a potent prohormone convertase inhibitor. Biochem. J. *307*, 689–695.

Johansson, M.K., Cook, R.M., Xu, J., and Raymond, K.N. (2004). Time gating improves sensitivity in energy transfer assays with terbium chelate/dark quencher oligonucleotide probes. J. Am. Chem. Soc. *126*, 16451–16455.

Kao, R.Y., To, A.P., Ng, L.W., Tsui, W.H., Lee, T.S., Tsoi, H.W., and Yuen, K.Y. (2004a). Characterization of SARS-CoV main protease and identification of biologically active small molecule inhibitors using a continuous fluorescence-based assay. FEBS Lett. *576*, 325–330.

Kao, R.Y., Tsui, W.H., Lee, T.S., Tanner, J.A., Watt, R.M., Huang, J.D., Hu, L., Chen, G., Chen, Z., Zhang, L., et al. (2004b). Identification of novel small-molecule inhibitors of severe acute respiratory syndrome-associated coronavirus by chemical genetics. Chem. Biol. *11*, 1293–1299.

Ksiazek, T.G., Erdman, D., Goldsmith, C.S., Zaki, S.R., Peret, T., Emery, S., Tong, S., Urbani, C., Comer, J.A., Lim, W., et al. (2003). A novel coronavirus associated with severe acute respiratory syndrome. N. Engl. J. Med. *348*, 1953–1966.

Kuang, W.F., Chow, L.P., Wu, M.H., and Hwang, L.H. (2005). Mutational and inhibitive analysis of SARS coronavirus 3C-like protease by fluorescence resonance energy transfer-based assays. Biochem. Biophys. Res. Commun. *331*, 1554–1559.

Kuo, C.J., Chi, Y.H., Hsu, J.T., and Liang, P.H. (2004). Characterization of SARS main protease and inhibitor assay using a fluorogenic substrate. Biochem. Biophys. Res. Commun. *318*, 862–867.

Liang, P.H. (2006). Characterization and inhibition of SARS-coronavirus main protease. Curr. Top. Med. Chem. *6*, 361–376.

Lindner, H.A., Fotouhi-Ardakani, N., Lytvyn, V., Lachance, P., Sulea, T., and Menard, R. (2005) The papain-like protease from the severe acute respiratory syndrome coronavirus is a deubiquitinating enzyme. J. Virol. *79*, 15199–208.

Liu, Y.C., Huang, V., Chao, T.C., Hsiao, C.D., Lin, A., Chang, M.F. and Chow, L.P. (2005). Screening of drugs by FRET analysis identifies inhibitors of SARS-CoV 3CL protease. Biochem. Biophys. Res. Commun. *333*, 194–199.

Marra, M.A., Jones, S.J., Astell, C.R., Holt, R.A., Brooks-Wilson, A., Butterfield, Y.S., Khattra, J., Asano, J.K., Barber, S.A., Chan, S.Y., et al. (2003). The genome sequence of the SARS-associated coronavirus. Science *300*, 1399–1404.

Moreira, B.G., You, Y., Behlke, M.A., and Owczarzy, R. (2005). Effects of fluorescent dyes, quenchers, and dangling ends on DNA duplex stability. Biochem. Biophys. Res. Commun. *327*, 473–484.

Newman, D.J. and Cragg, G.M. (2004). Marine natural products and related compounds in clinical and advanced preclinical trials. J. Nat. Prod. *67*, 1216–1238.

Patil, A.D., Kokke, W.C., Cochran, S., Francis, T.A., Tomszek, T., and Westley, J.W. (1992). Brominated polyacetylenic acids from the marine sponge *Xestospongia muta*: inhibitors of HIV protease. J. Nat. Prod. *55*, 1170–1177.

Richer, M.J., Juliano, L., Hashimoto, C., and Jean, F. (2004). Serpin mechanism of hepatitis C virus nonstructural 3 (NS3) protease inhibition: induced fit as a mechanism for narrow specificity. J. Biol. Chem. *279*, 10222–10227.

Rota, P.A., Oberste, M.S., Monroe, S.S., Nix, W.A., Campagnoli, R., Icenogle, J.P., Penaranda, S., Bankamp, B., Maher, K., Chen, M.H., et al. (2003). Characterization of a novel coronavirus associated with severe acute respiratory syndrome. Science *300*, 1394–1399.

Shi, J., Wei, Z., and Song, J. (2004). Dissection study on the severe acute respiratory syndrome 3C-like protease reveals the critical role of the extra domain in dimerization of the enzyme: defining the extra domain as a new target for design of highly specific protease inhibitors. J. Biol. Chem. *279*, 24765–24773.

Snijder, E.J., Bredenbeek, P.J., Dobbe, J.C., Thiel, V., Ziebuhr, J., Poon, L.L., Guan, Y., Rozanov, M., Spaan, W.J., and Gorbalenya, A.E. (2003). Unique and conserved features of genome and proteome of SARS-coronavirus, an early split-off from the coronavirus group 2 lineage. J. Mol. Biol. *331*, 991–1004.

Snijder, E.J., van der Meer, Y., Zevenhoven-Dobbe, J., Onderwater, J.J., van der Meulen, J., Koerten, H.K., and Mommaas, A.M. (2006) Ultrastructure and origin of membrane vesicles associated with the severe acute respiratory syndrome coronavirus replication complex. J. Virol. *80*, 5927–40.

Thiel, V., Ivanov, K.A., Putics, A., Hertzig, T., Schelle, B., Bayer, S., Weissbrich, B., Snijder, E.J., Rabenau, H., Doerr, H.W., et al. (2003). Mechanisms and enzymes involved in SARS coronavirus genome expression. J. Gen. Virol. *84*, 2305–2315.

Wilson, R. and Johansson, M.K. (2003). Photoluminescence and electrochemiluminescence of a Ru(II)(bpy)3-quencher dual-labeled oligonucleotide probe. Chem. Commun. (Camb.) *2003*, 2710–2711.

Yang, H., Yang, M., Ding, Y., Liu, Y., Lou, Z., Zhou, Z., Sun, L., Mo, L., Ye, S., Pang, H., et al. (2003). The crystal structures of severe acute respiratory syndrome virus main protease and its complex with an inhibitor. Proc. Natl. Acad. Sci. USA *100*, 13190–13195.

Yount, B., Curtis, K.M., Fritz, E.A., Hensley, L.E., Jahrling, P.B., Prentice, E., Denison, M.R., Geisbert, T.W., and Baric, R.S. (2003). Reverse genetics with a full-length infectious cDNA of severe acute respiratory syndrome coronavirus. Proc. Natl. Acad. Sci. USA *100*, 12995–13000.

Ziebuhr, J. (2004). Molecular biology of severe acute respiratory syndrome coronavirus. Curr. Opin. Microbiol. *7*, 412–419.

Received January 20, 2006; accepted June 13, 2006